DEM modelling of sequential fragmentation of zeolite granules under oedometric compression based on XCT observations

Pei Wang[a,*], Zeynep Karatza[b], Chloé Arson[a]

[a]*School of Civil and Environmental Engineering, Georgia Institute of Technology, USA*
[b]*School of Engineering, The University of Edinburgh, Edinburgh, UK*

Abstract

The objective of our research is to define a new Discrete Element Method (DEM) that can describe the processes involved in particle breakage and the resulting macroscopic behaviour of the particulate assembly, by directly observing and characterizing breakage mechanisms. To this aim, an oedometer compression test is performed on a dry granular assembly of zeolite, while acquiring 3D images of the specimen at several strain levels with an x-ray computed tomography device. We construct a DEM model that reproduces experimental observations, mainly: axial splitting is the main breakage mode; fragments are subjected to further breakage; very few fragments pass through the breakage plane. A fragment size limit is defined to reduce the computational cost associated with large numbers of breakage generations. We simulate the oedometer test for the same initial microstructure as in the lab test and with realistic particle mechanical properties, and compare the re-

*Corresponding author.
E-mail address: peiwang@gatech.edu
Fax: 404-385-0143

sults to the 3D images. The numerical results show that our proposed model can capture the size evolution, shape change and mechanical response of the tested specimens.
Keywords: oedometer test, X-ray Computed Tomography, particle breakage, DEM, breakage mechanics, image processing

1. Introduction

Particle breakage is the process by which grains divide up into smaller fragments due to high contact forces. Particle breakage can occur over a wide range of grain sizes, from fine sands to large size rock-fills, and results in changes in the magnitude and direction of contact forces in the granular assembly, and further, in the particle size distribution (PSD). At the macroscopic scale, particle breakage influences the mechanical behaviour, the porosity and the permeability of the granular assembly [1].

Experimental studies commonly focus on particle breakage and its effect on the material properties. It is claimed that the yielding along the normal compression line in the plot of void ratio vs. the logarithm of stress marks the onset of sand particle crushing, beyond which substantial breakage happens [2]. Lade and collaborators used the total energy input to predict particle breakage and established a relationship between the permeability of a granular assembly and the breakage factor, a scalar that quantifies the percentage of broken particles [3]. Multiple studies indicate a reduction of permeability with particle breakage [4, 5, 6]. Ovalle and collaborators conducted triaxial tests of large rock-fill samples to investigate their mechanical properties and found that particle strength is positively related to the sample-scale shear

strength [7].

The use of X-ray Computed Tomography (XCT) in experimental studies has allowed the 3D observation and measurement of the micro-mechanisms leading to particle breakage. Through single-particle compression tests, Zhao and collaborators observed the strong influence of particle morphology on particle stress distribution [8]. They found that particles with small radii of curvature were prone to extensive fragmentation, due to local stress concentrations at the contact points between the particle and the loading plates. The importance of using 3D images to describe particle morphology has been discussed in [9], showing that 2D and 3D measurements produce important differences in various particle shape parameters. XCT coupled with sophisticated algorithms, such as particle tracking [10], was used to predict and measure the life expectancy of porous granular materials during oedometric compression [11]. 3D images were also used for qualitative comparison of particle crushing with the DEM and the Finite Element Method (FEM) [12, 13].

Particle breakage was also studied theoretically using continuum mechanics. During the crushing process, the total input energy from external loading turns into elastic energy, breakage energy and redistribution energy [14, 15, 16]. Particle breakage is usually modelled by relating energy dissipation to the increase of particles' surface and/or to the frictional displacement field [17, 18, 19]. For instance, McDowell and Bolton followed a critical state soil mechanics approach and introduced particle breakage by defining the total particle surface and its increment as internal variables [20]. In the breakage mechanics theory [21, 22, 23, 24], the breakage energy and

the redistribution energy are fully coupled and the evolution of particle size distribution can be obtained. Breakage mechanics can be used to study the mechanical behaviour of crushable granular materials and extended to model creep, cementation and permeability changes.

In the past recent years, the DEM was used to simulate granular crushing [25, 26, 27, 28]. DEM models of single particle breakage can cover a wide range of particle sizes, from sand particles to railway ballast or even larger rocks [29, 30]. McDowell and Harireche found that particle size effects could be characterized using Weibull statistics [31]. Ueda et al. modelled the one-dimensional compression behaviour of assemblies of grains of various shapes [32]. They classified crushing processes into: cleavage destruction, bending fracture and edge abrasion. The occurrence rates of each of those processes are related to the particle shape. Wang and Arson analysed the shielding and size effects on single particle crushing, which yielded an empirical relationship between the coordination number and tensile strength, stressing the importance of porosity on tensile strength [33]. The DEM can also be used to model odeometer, shear or cone penetration tests, in which extensive breakage occurs [34, 35, 36]. Two main strategies exist in DEM to model particle breakage, *i.e.*, the cluster and the replacement methods. The cluster method is usually computationally more expensive as it requires a higher number of particles to be simulated, especially in large scale modelling. In the replacement method, it is important to select an appropriate breakage model to define the particle strength and size, the breakage planes and the position of the fragments. Particle breakage can also be modelled by combining the DEM with the FEM, the Scaled Boundary Finite Element Method (SBFEM)

and the eXtended Finite Element Method (XFEM) [37, 38, 39, 40, 41, 27]. In these methods, grain-to-grain interactions are simulated with the DEM, and after each step of the DEM calculation, particles are analysed separately to determine the breakage status. The above combined methods are very similar to DEM cluster methods in that they require pre-generating elements (FEM elements) in each crushable particle and can produce angular fragments after breakage.

The objective of this research is to build a new DEM breakage model, using direct micro-scale observations and measurements from 3D images, to realistically represent the breakage process and capture the resulting macroscopic material properties. To achieve this goal, we first conducted an oedometer test on dry, uniform zeolite specimens and used XCT to scan the specimen at different stress levels. We used several image processing algorithms to identify and track intact particles and fragments and get information about the evolution of grading and about the types of breakage events. Our observations are reported in Section 2. Then we reviewed DEM breakage models based on the replacement method and we proposed a new robust model, which can simulate sequential breakage, generate non-spherical fragments and predict appropriate arrangements of fragments. Our new proposed model is explained in Section 3. Lastly, we calibrated the parameters and simulated the oedometer test. The results and simulations, presented in Section 4, show good agreement with the experimental results.

2. Zeolite oedometer test and XCT

2.1. Experimental methods

For this study, industrially manufactured zeolite granules were tested under strain-controlled oedometric compression and scanned by XCT. The material was chosen due to its highly spherical and rounded shape, which facilitates the modelling of the experimental procedure using the DEM. Each particle had a density of 2.18 g/cm^3 and a crushing strength of 15 N according to the supplier's specifications. The intact sample had a mean particle diameter (D_{50}) of 1.36 mm and a very uniform grading ($C_u = 1.07$, $C_u = \frac{D_{60}}{D_{10}}$). The specimens were created to have the same repeatable dense initial configuration (porosity 40 %) by pluviation. The large particle size and the uniform grading allowed all intact particles to be imaged with the same level of detail. A particle's fracture probability is strongly dependent on the relative size of its nearest neighbours; particles with neighbours of the same size are most likely to fracture, while the relatively larger particles get cushioned from the smallest neighbours as they continue to break [42, 43]. Therefore, the sample was sieved to a very narrow grading to ensure the highest possible probability of fracturing. The specimen had a diameter of 15 mm and a target height of 15 mm. The oedometric cell (specially designed for this study) was made of PEEK (PolyEther Ether Ketone), chosen for its low x-ray absorption and low friction properties [more details can be found in 44]. The loading direction was ascending and the quasi-static loading was performed with an axial loading rate of 50 µm/min.

XCT was performed in Laboratoire 3SR (Grenoble, France) with an x-ray scanner using 100 kV of acceleration [described in 45]. Figure 1 shows

a schematic of the apparatus and an annotated picture of the XCT set-up. The voxel size (*i.e.*, 3D pixel) was 12.3 µm/px, which allowed getting images of high resolution. Loading was performed *in-situ* in the scanner under displacement control, setting the strain rate to zero during scanning (*i.e.*, loading stage).

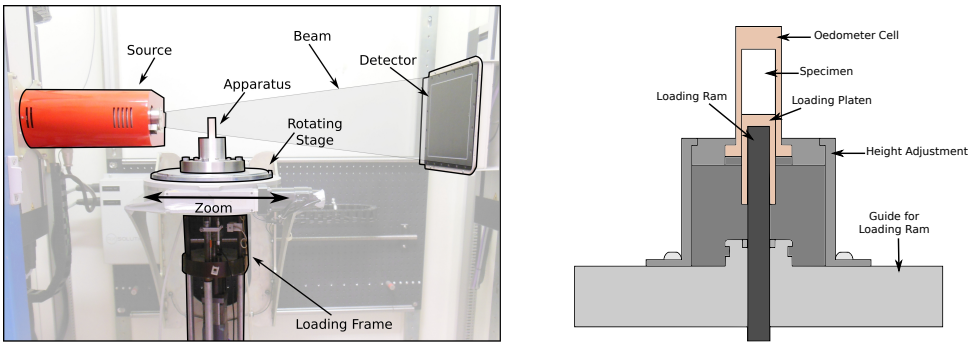

Figure 1: Left: Annotated image of XCT set up (i.e. apparatus placed in x-ray cabin); Right: schematic of oedometric apparatus.

2.2. Analysis of particle breakage using XCT

A 3D reconstruction provided full microstructure information in the form of 32-bit floating points. In order to save space and have some inherent normalisation between the scans, the data was degraded to a 16-bit integer format, which offers a 2^{16} dynamic range of grey scale information and is more than the noise of reconstruction. Figure 2 shows vertical slices from the reconstructed 16-bit 3D images. In the first loading stages, only primary breakage appears to occur, however after an axial strain of 7.12 %, a number of fragments undergo significant breakage. Additionally, from a careful visual inspection of the images, the majority of breakage events occur close to the

moving boundaries, as previously observed in [46].

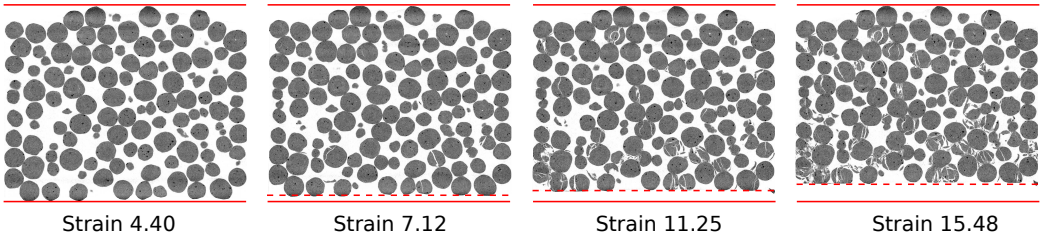

Figure 2: Vertical 2D slices from the experimental oedometer test (strains in %)

For the measurement of the volume, size and shape of the particles, the particles must first be detected, therefore the continuous grey scale information must be segmented. To do so, we used an algorithm that preserves moments [47] to set a threshold that distinguishes the solid and void phases (*i.e.*, binary image). We applied a watershed analysis [48] to separate contacting particles, so that each particle is surrounded by voxels that represent void, allowing individual particle measurements to be performed. A commercial software (Visilog) [49] was used for all the segmentations in this work.

Intra-granular porosity can lead to over-segmented grains (*i.e.* intact particles get split into several particles), hence careful binarisation is a key feature for further segmentation. Zeolite particles have significant intra-porosity, which was filtered after the initial binarisation, to avoid over-segmentation. The internal pores were significantly smaller and more spherical than the inter-particulate pores, which provided a basis to define the criterion in the filtering process. This procedure is described in Figure 3. Provided the limitations of the segmentation technique, for the total amount of breakage that we generated up to an axial strain of 15.48 %, we could confidently detect

particles down to a resolution of 0.2 mm. This value is set as the ultimate fragment size in the DEM analysis presented in the following.

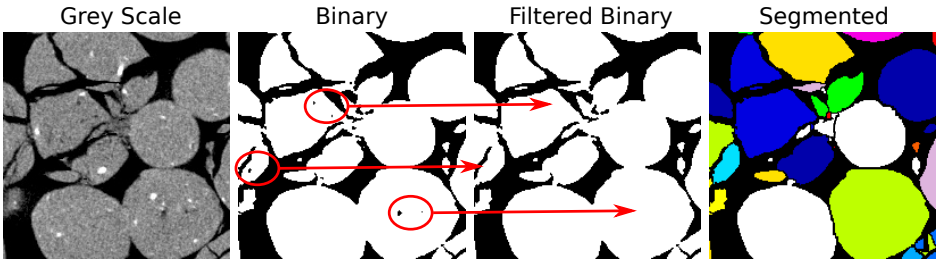

Figure 3: Identifying and filtering intra-particle porosity.

After each particle (intact or fragment) has been identified, we measure the perpendicular maximum D_{max} and minimum D_{min} lengths of the particle at 60 different orientations. Then the medium diameter D_{med} of a prescribed ellipsoid of same volume as the particle is calculated and assigned to each particle and used to get the PSD for each loading stage [50]. The flatness ratio and the aspect ratio, respectively given by $FR = D_{min}/D_{med}$ and $AR = D_{max}/D_{min}$, can then be obtained.

3. DEM particle breakage model

In DEM, particle breakage can be modelled using the cluster method (with breakable agglomerates) or the replacement method. In the former, crushable particles are represented by a cluster of smaller elements that are bonded together. The cluster breaks when stresses in the bonds exceed the corresponding bond strengths. The cluster method was used in many instances [30, 51, 34]. In the replacement method, breakage occurs when the total stress induced from contacting particles is larger than the particle

strength. The broken particle is then replaced by several smaller fragments. In the cluster method, micro-cracks that occur in a particle before a major breakage event can be tracked by the number of broken bonds. The shape of fragments truly depends on the stress distribution in the crushable particle, but the solution depends on the number of elements and bonds considered in the cluster. Precise models are computationally expensive due to the large number of elements represented in each cluster (typically, several tens of thousands of elements per cluster). The replacement method is relatively more effective because the number of elements is equal to the number of particles. The replacement method can be used to analyse driving forces, breakage modes and the effect of coordination number on crushing. The aforementioned reasons justify the choice of the replacement method in our simulations. The main challenge in the replacement method is the definition of the breakage model parameters, such as the particle strength, the position and orientation of breakage planes and the number and size of fragments.

In this section, we first review existing replacement models. Then we propose a new model that can simulate sequential breakage, generate non-spherical fragments and predict appropriate fragment arrangements. We then use this model to simulate the oedometer test presented in section 2.

3.1. A review of current replacement models

In the replacement method, the breakage criterion, *i.e.,* the limit condition of the crushable particle, needs to be defined in terms of pressure, tensile strength, shear strength, or maximum contact force, depending on the breakage mechanism. This limit condition can be defined by a single value or by a variable that follows a statistical distribution [52, 53]. Due to the difficulty

in obtaining the stress distribution in a particle subjected to several contact forces, the following simplified stress averaging method is often adopted [54]:

$$\sigma_{ij} = \frac{1}{V} \sum_{N_c} (x_i^{(c)} - x_i^{(p)}) F_j^{(c,p)} \tag{1}$$

where V is the volume of the particle, N_c is the total number of contacts, $x^{(c)}$ and $x^{(p)}$ are the locations of the contact and particle centroid, respectively, and $F_j^{(c,p)}$ is the force acting on the particle at the j^{th} contact.

Åström and Herrmann compared two different limit conditions for breakage, the mean stress and the largest compressive contact force. They found that using mean stress as a criterion led to unstable breakage. Contrarily, a criterion based on the largest compressive force predicts stable breakage mechanisms and more accurate PSDs [55]. However, the authors did not provide the expression of the average contact force that they used in the pressure method, neither did they calibrate the numerical results against experiments. In another study, the arithmetic mean of the normal component of the contact force, $\bar{F}_n$, was compared to a critical force magnitude, F^*_{crit}, and a grain crushed when $\bar{F}_n > F^*_{crit}$ [56]. By investigating two breakage criteria and several configurations of post-crushing replacement, it was concluded that the expected ultimate fractal distribution of particle sizes could be approached irrespective of the breakage criterion used.

Ciantia and collaborators used the maximum normal contact force in the limiting criterion $F \leq \sigma_{lim} A_F = F_{lim}$, where F is the maximum normal contact force, σ_{lim} is the limit strength and A_F is the contact area [53]. 3D simulations of an oedometer test showed that this criterion was computationally efficient and accurate. A criterion expressed in maximum contact force

was also used in [57], and later this criterion proved to better represent the PSD evolution and the average stress distribution [54]. Zhu and Zhao [58] examined existing crushing criteria by crushing a single sand particle using the peridynamic method, and results show that a particle breaks when the maximum contact force reaches a certain threshold.

In most single particle compression tests, breakage was found to be caused by the tensile stress, splitting the grain axially, like in a Brazilian test [59]. According to Tsongui and collaborators [60], when a grain is in contact with several neighbours, the tensile stress at the centre is close to $(\sigma_1 - 3\sigma_3)/2$. After simulating an oedometric compression test in 2D with the DEM, using $(\sigma_1 - 3\sigma_3)/2$ as the failure criterion, a good agreement was found with the 2D experimental results.

In another approach, McDowell and collaborators defined the breakage criterion in terms of octahedral shear stress, $q = 1/3[(\sigma_1 - \sigma_2)^2 + (\sigma_2 - \sigma_3)^2 + (\sigma_1 - \sigma_3)^2]^{1/2}$ [61]. They proposed that it would be unlikely for a particle to break when it is subjected to a high isotropic stress, and that, therefore, the deviatoric stress played a more important role in breakage. They used the model to simulate the isotropic compression of silica sand and achieved a normal compression line of the same slope as in experimental results from a 1D compression test.

Once the breakage threshold is reached, the crushable particle is replaced by smaller elements that represent the fragments. Different fragmentation methods were proposed, based on mass conservation, PSD evolution and various breakage mechanisms. McDowell and de Bono introduced two equally sized spheres to replace the broken particle, without mass loss, as shown in

Figure 4(a) [62]. The axis joining the two centres is in the direction of the minor principal stress, which is similar to the breakage configuration in a single particle compression test. However, the main problem in this method is the development of a high elastic stress due to the overlap of the particles. Assuming that particle breakage is the result of tensile failure, Lobo-Guerrero and collaborators used a group of eight particles to replace the broken particle [63]. The axis joining the two largest fragments is perpendicular to the direction of maximum contact force, see Figure 4(b). Ben-Nun and Einav studied particle breakage in three configurations, one of which is shown in Figure 4(c). In all three methods, they obtained a PSD that obeyed a power-law, scaling with three different fractal dimensions [64]. In terms of 3D simulations, Ciantia and collaborators conducted a parametric study on the effect of the splitting configuration and found that the mechanical response does not change significantly when there are more than 14 spheres in the fragments. The configuration of the 14-sphere replacement method, shown in Figure 4(d), is also based on the observation of breakage of a single particle subjected to diametric loads.

In summary, the maximum contact force method yields the best results and has been recently accepted by researchers as the most appropriate breakage criterion. Although this method seems biased due to the absence of account for the coordination number or the spacial distribution of contact forces, it ensures that small particles are more likely to break while large particles are protected by smaller ones, which is usually true in experiments [54]. In terms of fragment geometric arrangement, previous configurations share some interesting similarities: fragments are separate (no bond connec-

tion), have a disc shape (spherical shape in 3D) and there are fragments passing through the breakage plane. From the test we conducted in Section 2 and previous studies in [65, 60], fragments of broken particles remain close to their mother particles. While in the breakage models mentioned earlier, where there are no bonds among fragments, spheres have much less interlocking than real angular fragments observed in experiments [66]. Unbonded fragments thus undergo large displacements away from their mother particle's position. In addition, it is also clear that for both axial splitting and multi-fragmentation in our tests, none or very few fragments pass through the breakage plane, while contacts always do. The last observations, which contradict previous fragment configurations, made us think of a more realistic arrangement of fragments to model particle breakage.

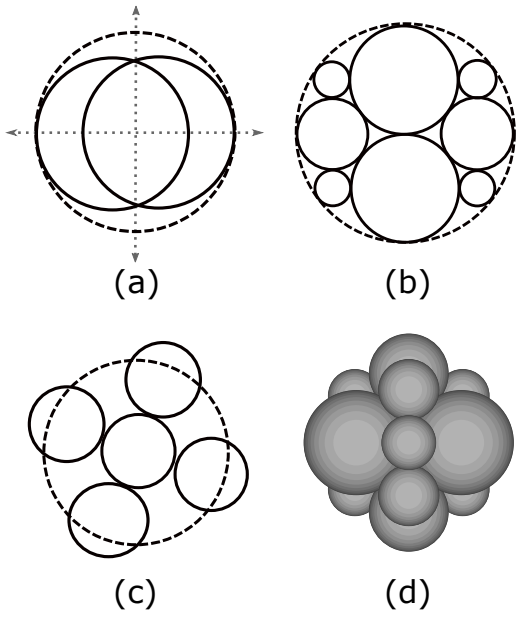

Figure 4: Examples of fragment arrangements [62, 63, 64, 35]

3.2. A new replacement model

To overcome the shortcomings of the breakage models discussed in Section 3.1, we propose a new replacement method that: (1) contains angular fragments made of bonded spherical particles; (2) considers multiple generations of breakage (including both grain breakage and bond breakage); and (3) does not generate fragments on the failure plane. As discussed in Section 3.1, we used the maximum contact force as the breakage criterion in our replacement model. During the simulation, the maximum contact force (F_{max}) of each particle is monitored. When the stress defined as $\sigma_{F_{max}} = F_{max}/d^2$ exceeds the grain strength, the particle is then defined as being broken. The choice of the model parameters is discussed in the following.

After a particle is identified as being broken, the next step is to replace it with smaller fragments. We focus on breakage mechanisms where a major splitting event occurs first, during which the particle is separated into two fragments along a plane that contains the contact points with the largest contact forces. During the splitting event, the elastic energy stored in the breaking particle is released and partially turns into fragment kinetic energy. The fragments move in the least confined direction, the largest contact forces (contained in the splitting plane) decrease, and smaller contact forces ("confining" forces) increase. This latter phenomenon leads to secondary breakage in the fragments, as shown in Figure 5. The rearrangement of fragments ultimately transforms kinetic energy into heat and another state of equilibrium is reached. This micro-mechanism of particle breakage is validated from the observation that most broken particles undergo a primary axial splitting and that secondary failure occurs in the fragments.

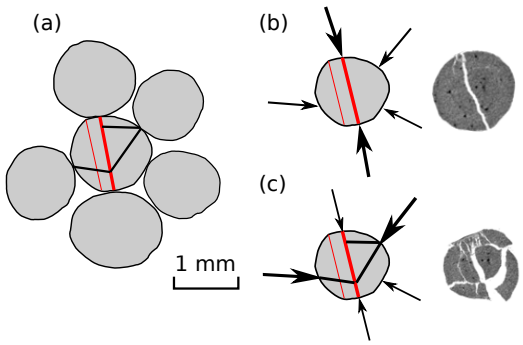

Figure 5: Sketch of the sequential breakage mechanism in a zeolite particle (thicker arrows indicate larger contact forces) (a) local assembly of particles in the zeolite sample before breakage; (b) first generation of breakage (represented by a red line); (c) sequential breakage (represented by black lines)

To model the primary splitting event, we propose to replace the crushable particle by two fragments modelled by clusters of 17 bonded rigid spherical elements (1 central sphere surrounded by 16 smaller spheres of two different sizes) as sketched in Figure 6. The 16 smaller spheres are tangent to the sphere that formed the mother particle. The number of elementary spheres in each cluster that represents a fragment was chosen so as to limit volume loss and ensure computational efficiency. Less volume is lost when replacing a particle by its fragments when the clusters contain a large number of small spherical elements. With clusters of 17 particles, the volume loss is of 46 %, which, according to Ciantia and collaborators [53], is below the critical volume loss (47 %) above which the DEM model cannot represent the physical experiment. Clusters are breakable, which allows capturing secondary breakage in the DEM simulations. Spheres in the same fragment are connected together with parallel bonds, which are joints that transmit forces and mo-

ments [67]. Secondary breakage triggers when the bond breakage criterion is exceeded. It is important to arrange the spheres in appropriate positions so that the replacement process can match the breakage mechanism to its maximum extent. The arrangement is determined by the breakage plane. In a 2D simulation, σ_3 is zero according to Equation 1, thus the breakage occurs along a line that passes through the centre of the mother particle and is coaxial with the maximum principal stress or maximum contact force [62, 60]. In 3D we need two vectors to define the plane direction. If these vectors are defined as the two largest principal directions $\bar{n}_1$ and $\bar{n}_2$ (e.g., [54, 62]), the maximum contact force is not guaranteed to be on the splitting plane. To overcome this limitation, Ciantia rotated the replacement configuration twice so that the vertical axis in the configuration becomes parallel to the direction of contact force [53, 68, 35]. However, this rotation was not justified by any physical or mechanical explanation. When a particle breaks, fracture propagates in the direction perpendicular to the minimum principal stress direction. In addition, according to our experiments, the breakage planes of broken particles do pass through the contact points. Therefore, in our simulations, we assume that the breakage plane passes through the contact with maximum contact force and that it is perpendicular to the plane that contains the directions of σ_3 and of the maximum normal contact force.

Additionally, we need to set the smallest particle size allowed to break, to avoid high computational cost. Theoretically, the isolated spherical grains can always break when the breakage criterion is met. However, the large gap between the relative mass of the particles will greatly increase computational time because the critical time step in DEM is calculated as $t_{crit} = \sqrt{m/k}$,

where m is the mass of the smallest grain and k is its stiffness. We set the smallest breakable particle size to be 0.2 mm, which is the smallest size that can be identified from grain segmentation in XCT image analysis. Consequently particles below this size threshold do not break in our simulations. Figure 6 explains how sequential breakage is represented in our proposed DEM model. The calibration of the new breakage model is discussed in the following section.

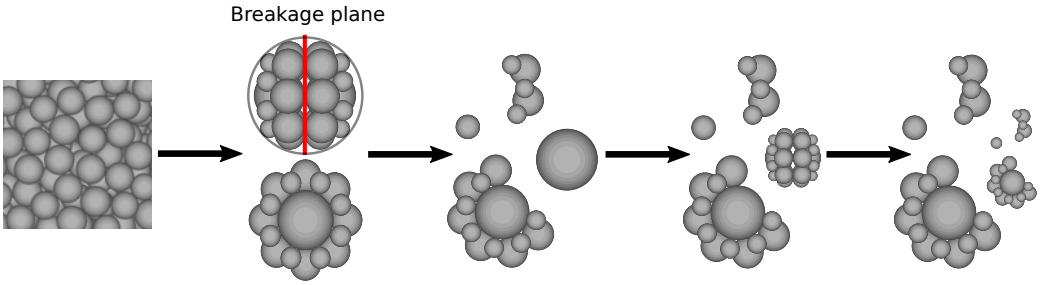

Figure 6: Schematic of multiple generations of breakage modelled with the new DEM replacement method

4. DEM simulation of the oedometer test

4.1. A brief introduction of the DEM and of the contact model

The DEM was initially proposed by Cundall and Strack in 1970s to investigate the behaviour of granular assemblies [69]. In this method, the interactions of particles are determined by contacts and movements are governed by Newton's second law. Simulations in this research are conducted with PFC3D DEM sofware. Rigid spheres and rigid walls are allowed to overlap at contacts. Contact surface areas are small compared to the size

of the spherical elements. Spheres can be bonded together to form clusters of different sizes and shapes. Therefore, contact behaviours are governed by three constitutive laws: a stiffness model; a slip model; and a bonding model [70]. The stiffness model provides a relationship between a contact force and a relative displacement. The slip model defines the maximum shear force that can build up at a contact before a slip movement occurs. The bonding model characterizes the rheology of bonds, which can undertake force or bending moments. Crack propagation is often represented by bond breakage, in which case, bonds disappear during the simulation.

We used the Hertz-Mindlin stiffness model in which the normal and shear stiffnesses increase with the sphere overlap [70]. The two governing parameters are the shear modulus G and Poisson's ratio ν. In the slip model, the maximum shear force at a contact is expressed as $F^s_{max} = \mu|F^n_i|$, where μ is the friction coefficient and F^n_i is the normal contact force. We used the parallel bond model, in which bonds between balls are represented as short beams of circular cross-section. Parallel bonds can transmit both forces and moments between particles, and a detailed description of this model can be found in [70].

4.2. DEM model construction and calibration

We modelled the oedometer compression test on zeolite granules using the replacement model proposed in Section 3.2. The parameters in the model are the particles' shear modulus (G) and Poisson ratio (ν), the strength of particles of average size d_0 (σ_{t0}), the Weibull modulus (m), the normal and shear bond strengths ($\bar{\sigma}_n$ and $\bar{\sigma}_t$), the parallel bond normal and shear stiffnesses ($\bar{k}^n$ and $\bar{k}^s$) and the parallel bond radius multiplier λ.

The contact between unbonded spherical particles is governed by the Hertzian contact model, in which the behaviour is solely defined by the shear modulus (G) and Poisson's ratio (ν). They are chosen to match the properties of zeolite. We assume that splitting is caused by tensile failure and the relationship between tensile strength and maximum contact force is characterized by $\sigma_{F_{max}} = F_{max}/d^2$, where d is the diameter of the particle [59, 71]. In a single particle compression test, the grain strength is the particle's tensile strength. However, in a granular assembly, each grain is shielded by its neighbours, leading to a redistribution of the stress induced by contact forces that results in quasi-hydrostatic stress and reduced tensile stress. In both experiments and simulations, it is reported that the force necessary to break a particle within a granular assembly is several times higher than that necessary to break an unconfined particle [33, 72]. In our simulations, the average coordination number of the particles was about 5.3. According to the 2D simulations presented in [72], grain tensile strength for that coordination number is about 3 times higher than that measured during a uniaxial tensile splitting test (3.3 MPa for zeolite grains). Our simulations being in 3D, the best fit with experimental results was found for a particle tensile strength $\sigma_{t0} = 12.0$ MPa, which is slightly higher than the recommended strength in 2D. In addition, a size effect was noted in a number of different materials [33, 73, 74, 75], indicating that materials with larger sized particles usually have lower strengths. We accounted for the size effect by using a Weibull distribution of tensile strength, where the survival probability of a particle of size d is given by $P(d) = exp[-(d/d_0)^3(\sigma_{F_{max}}/\sigma_{t0})^m]$ [76, 77], and we set the Weibull modulus to 3.0, which is a reasonable estimation,

according to the test results summarized in [77]. The parallel bonds' normal and shear strengths were set equal to 3.3 MPa, which corresponds to the tensile strength found from single particle crushing tests [44]. The parallel bonds' normal and shear stiffnesses were calculated using the equations $\bar{k}^n = E/(R^{(A)} + R^{(B)})$ and $\bar{k}^s = G/(R^{(A)} + R^{(B)})$, as proposed by [78]; where $R^{(A)}$ and $R^{(B)}$ are the radii of the bonded spheres and E the Young's modulus calculated from G and ν. The frictional coefficient, which is known to not greatly influence DEM results [44, 79], was set to 0.5; this is a common choice in DEM simulation [27, 78]. The parallel bonds' radius multiplier λ was used to define the radius of the cross-section of the parallel bonds; the larger it is the stronger the bond is (*i.e.*, a larger force is required to break the bond). The default value of this parameter is 1.0 in the parallel bond model, which means that the radius of the cross-section is the average of the radii of the two connected spheres. However, due to the volume loss in the replacement process, the contact area is underestimated in the simulation. The value of λ was fitted by trial and error to achieve the best match with the experimental macroscopic stress - strain curve. A summary of the parameters used in the simulation is shown in Table 1.

In order to reproduce the conditions of the experiment, the diameter and height of the sample were respectively set to 15 mm and 12.25 mm (same as in the experimental set-up). Particles were initially randomly generated in a cylinder that was 15 mm in diameter and 30 mm in height, and then subjected to free falling movement to the bottom of the cylinder. In order to generate particles following the same initial grading as in the experiment, we fitted the probability density of particle sizes found experimentally to a

Table 1: Parameters used in the DEM simulation

Shear modulus (G)	GPa	2.2
Possion's ratio (ν)	-	0.25
Density of sphere (ρ)	kg/m^3	2180
Material tensile strength (σ_{t0})	MPa	12.0
Weibull modulus (m)	-	3.0
Normal and shear bond strength ($\bar{\sigma}_n$ and $\bar{\sigma}_t$)	N/m^3	3.3
Frictional coefficient of sphere (μ)	-	0.5
Parallel bond radius multiplier (λ)	-	1.25

normal distribution and we used it to generate particles in the DEM sample. The probability density functions are shown in Figure 7. The porosity of the sample was between 44 % and 45 %, like in the physical test. The loading speed was set to 0.1 m/s and the time step was in the order of 10^{-8}s to 10^{-7}s, which allowed simulating quasi-static conditions [31, 33, 78]. During loading, the breakage criterion was checked every ten steps and the compressive strain of the assembly, the contact forces, the number of broken grains and the location of the particles were recorded. A flow chart that summarizes the simulation steps is shown in Figure 8.

4.3. Simulation results

The stress – strain curves for both the experiment and the simulation responses are shown in Figure 9, in which we can see that simulation results follow the same trend as the experimental ones. Note that the curves do not start at 0 strain because results were plotted starting at a stress of 100 MPa.

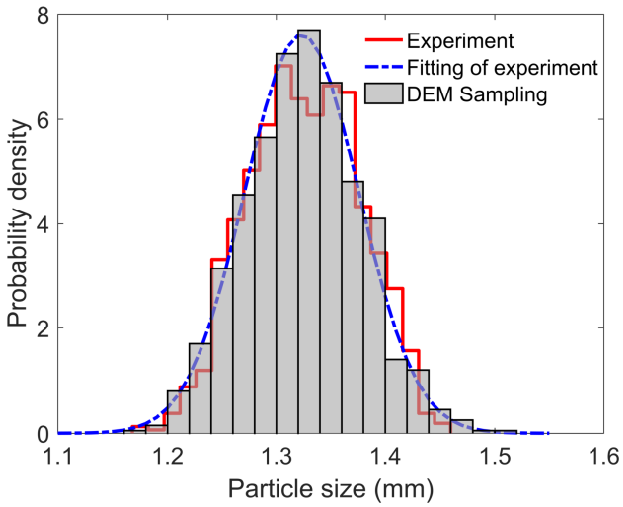

Figure 7: Probability density functions of DEM and experimental initial particle configurations (before oedometric compression)

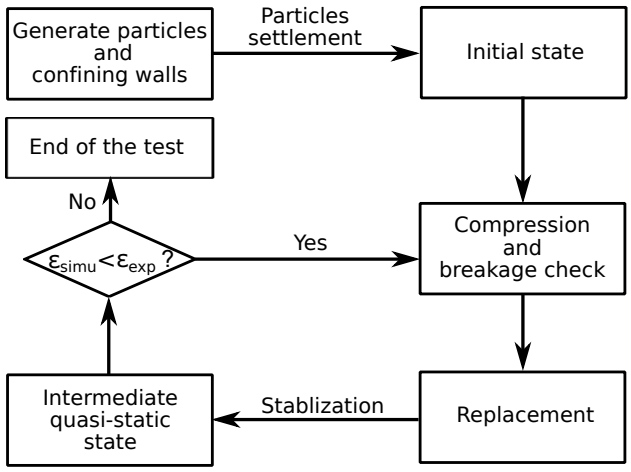

Figure 8: DEM simulation flow chart for the oedometer test

The stress – strain curve clearly shows a yielding region at around 2 MPa after the initial compaction. Before yielding, the curve is smooth with just a few fluctuations, indicating grain breakage and stress release due to particle rearrangement. After yielding, the curve shows important fluctuations caused by extensive particle and bond breakage. The rapid increase in the number of broken particles and bonds after yielding is more evident in Figure 10. Before yielding there are 20 broken particles and 300 broken bonds, yet the two values rapidly increase to respectively 280 and 10,000 as the compressive stress reaches 4 MPa. Figure 11 shows the sample before and after compression (note that in order to have a better view of the fragments, intact particles are set invisible in Figure 11(b)). We can also see that breakage is more likely to occur near the loading platens, which is in agreement with experimental observations.

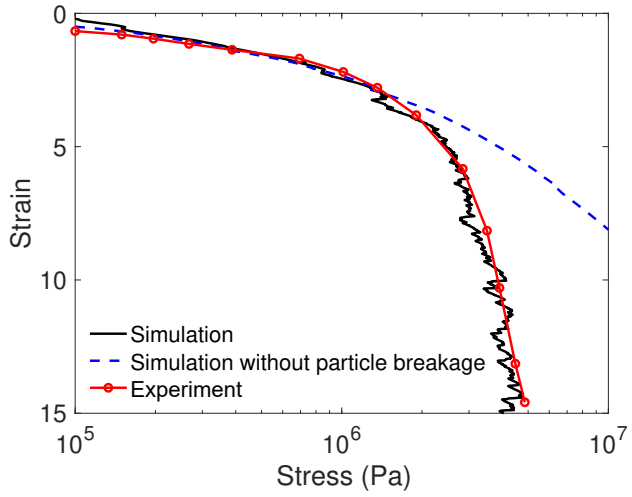

Figure 9: Comparison of DEM and experimental results of an oedometric compression test performed on zeolite

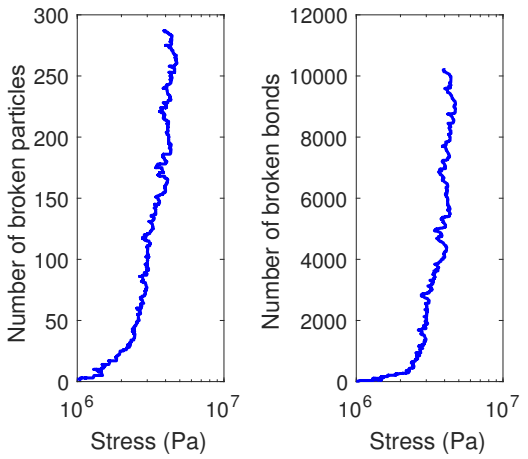

Figure 10: Number of broken particles and broken bonds at the end of the simulation

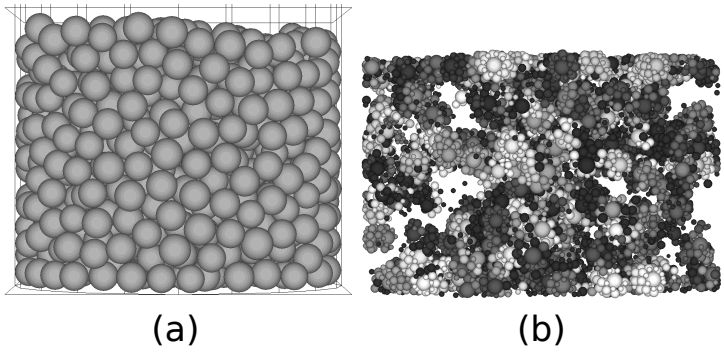

Figure 11: DEM model before compression (a) and broken particles after compression (b) [note that intact particles are set invisible in (b)]

We now focus on the evolution of the PSD during compression. Figure 12 compares the numerical and experimental PSDs at axial strains of 0.0%, 4.4%, 7.12%, 11.28% and 15.48%: DEM results are in agreement with physical measures. As the strain increases, particles continue to break, resulting in the increase of the number of fines. It is noticeable that the PSD curves in the DEM simulation are slightly below those in the experiment for the size range from 1.1 mm to 1.2 mm. We attribute this difference to the surface chipping that occurs during the experiment, which cannot be captured in this model. In fact, at the end of the simulation (i.e. for an axial strain of 15.48%), we find that 35% of the intact particles have broken, compared to nearly 70% in the experiment. That said, one has to keep in mind that most breakage models aim to only reproduce the macroscopic stress/strain curve and the PSD [80, 81, 82], which are both in agreement with experimental measures in our proposed model. We conclude that our new sequential breakage model is representative. Chipping will be studied in future work.

An important feature of our proposed new model is the generation of non-spherical fragments. We use the Flatness Ratio (FR) and the Aspect Ratio (AR) to characterize particles' shapes; these two parameters are given by $FR = D_{min}/D_{med}$ and $AR = D_{max}/D_{min}$, where D_{min}, D_{med}, and D_{max} are respectively the smallest, medium and largest dimensions of the smallest cube that can be circumscribed to a particle. The distributions of FR and AR calculated at the end of the simulations are shown in Figures 13 and 14, respectively. Note that in the initial test, both the FR and AR are equal to 1.0, because granules are initially quasi-spherical. At the end of the experiments (respectively, simulations), 81% of the particles (respectively,

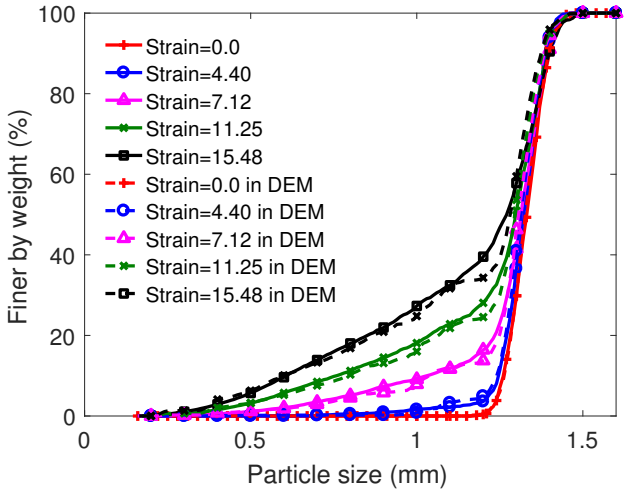

Figure 12: Evolution of the PSD in the simulation and in the experiments

78% of the particles) have an FR between 0.9 and 1.0 and 71% of the particles (respectively, of 80% the particles) have an AR in the range of 1.0 to 2.0. The match between experimental and numerical results is thus satisfactory for quasi-spherical fragments, which constitute about three-quarters of the particles in the final stage of the oedometer test. Figure 13 shows that the number of particles with an FR between 0.8 and 0.9 (respectively, between 0.4 and 0.8) is lower (respectively, higher) in the simulation than in the experiment. We think that the high number of particles with an FR between 0.8 and 0.9 in the experiment is due to chipping, a process by which mother particles that have not yet experienced primary breakage by splitting are eroded. Eroded mother particles are considered non-spherical in the image analysis but they are considered spherical in our model. Furthermore, the high number of particles with an FR between 0.4 and 0.8 in the simulations is attributed to the type of primary breakage in our model, which produces

fragments of FR around 0.5, separated by a breakage plane. Figure 14 shows that the number of particles with an AR between 2.0 and 3.0 (respectively, over 3.0) is lower than (respectively, negligible in front of) the experimental values. This difference is also attributed to chipping, which produces a large number of angular fragments (chips) through a process that is not captured (yet) by the proposed model. To support this interpretation, note that in the experiments, the smallest 10% particles (which stem in part from chipping) have, in average, an AR that is 14% higher than the 90% larger particles. An example of surface chipping is shown in Figure 15: the particle that is subject to surface chipping is surrounded by eight neighbouring particles. This process generated a large fragment with a FR close to 1.0 and several smaller fragments with high AR, which can explain the differences between the simulations and the experiment in Figures 13 and 14.

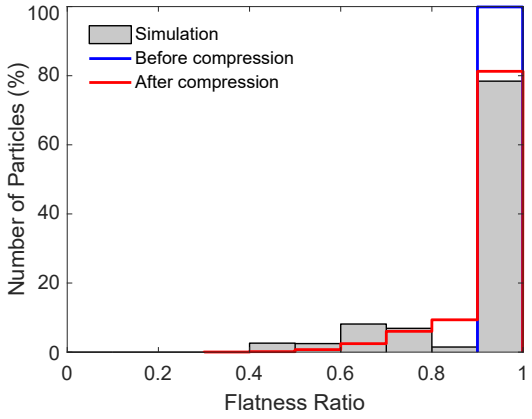

Figure 13: Flatness ratios of the particles before and after the compression

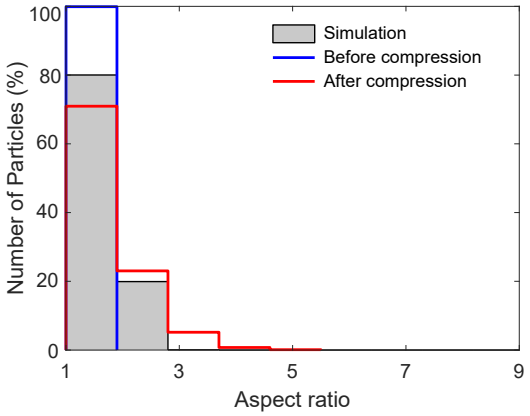

Figure 14: Aspect ratios of the particles before and after the compression

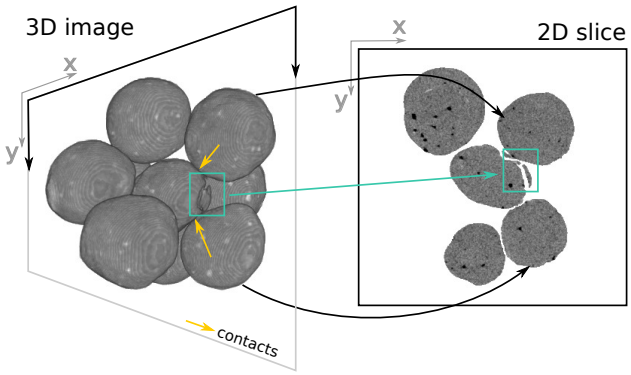

Figure 15: 3D image (left) and 2D slice (right) of a particle undergoing surface chipping (Contact delimiting the failure are denoted with yellow arrows) [83]

5. Conclusions

Understanding the micro-mechanisms leading to particle crushing is important because fragmentation affects the bulk mechanical behaviour of granular materials. The DEM is often used to study particle breakage. An appropriate breakage model is crucial in DEM because it defines the breakage criterion and the configuration of the fragments. In this paper, we conducted an oedometer test on zeolite granules and employed XCT during loading, and we proposed a new DEM replacement method. We analysed the experimental results and the 3D images at both sample and grain scales with emphasis given on particle breakage. From the quantitative 3D experimental analysis, we validated and calibrated the DEM results. In summary, here are the main conclusions:

1. The DEM model includes both tensile splitting and bond breakage, combining the two most commonly used DEM models in the literature: particle replacement (used for primary splitting breakage) and clustering (used for breakage of fragments). The model allows simulating several cycles of splitting breakage and cluster fragment breakage. Sequential breakage stops when a fragment reaches a critical size of 200 microns, which corresponds to the minimum segmentation size from XCT image analysis.
2. The use of the cluster method implies that angular fragments can be produced during the simulation, depicting a realistic evolution of particle grading during crushing.
3. An important improvement upon previously proposed models is that during tensile splitting, the breakage plane is defined by the contact

carrying the maximum normal force and by the direction of minimum principal stress, instead of assuming that the breakage plane contains the two maximum contact force vectors.

4. The 3D images confirm that multiple generations of breakage occur during the oedometric compression of zeolite and, by using rigorous algorithms, we could accurately quantify the evolution of the PSD. The PSD obtained with the new DEM model exhibited an impressive matching with experimental results.
5. The bulk response of the oedometric compression was also compared to the DEM results. Using the new breakage model results in good agreement with the experimental stress – strain relationship.

This research is expected to improve the breakage models used in DEM, to better represent the breakage process as well as the definition of macroscopic properties, and to provide a useful tool for further analysis of particle breakage mechanisms using the DEM.

6. Acknowledgements

The authors are grateful to the insightful discussions and support of Prof. Viggiani and Dr. Andò. Dr Karatza would like to thank Mr. Charrier for his valuable help during the XCT, Mr. Debove for helping create the oedometer, the UK Engineering and Physical Sciences Research Council (EPSRC) - DTP for the PhD studentship, the International Fine Particles Research Institute (IFPRI) for the financial support, and Dr Papanicolopulos and Prof. Ooi for their support.

References

[1] Y. Nakata, Y. Kato, M. Hyodo, A. F. HYDE, H. Murata, One-dimensional compression behaviour of uniformly graded sand related to single particle crushing strength, Soils and Foundations 41 (2) (2001) 39–51.

[2] G. McDowell, M. Bolton, On the micromechanics of crushable aggregates, Geotechnique 48 (5) (1998) 667–679.

[3] P. V. Lade, J. A. Yamamuro, P. A. Bopp, Significance of particle crushing in granular materials, Journal of Geotechnical Engineering 122 (4) (1996) 309–316.

[4] M. N. Panda, L. W. Lake, Estimation of single-phase permeability from parameters of particle-size distribution, AAPG bulletin 78 (7) (1994) 1028–1039.

[5] B. Crawford, D. Faulkner, E. Rutter, Strength, porosity, and permeability development during hydrostatic and shear loading of synthetic quartz-clay fault gouge, Journal of Geophysical Research: Solid Earth 113 (B3).

[6] E. Papamichos, I. Vardoulakis, H. Ouadfel, Permeability reduction due to grain crushing around a perforation, in: International Journal of Rock Mechanics and Mining Sciences & Geomechanics Abstracts, Vol. 30, Elsevier, 1993, pp. 1223–1229.

[7] C. Ovalle, E. Frossard, C. Dano, W. Hu, S. Maiolino, P.-Y. Hicher, The effect of size on the strength of coarse rock aggregates and large

rockfill samples through experimental data, Acta Mechanica 225 (8) (2014) 2199–2216.

[8] B. Zhao, J. Wang, M. R. Coop, G. Viggiani, M. Jiang, An investigation of single sand particle fracture using x-ray micro-tomography., Géotechnique 65 (8) (2015) 625 – 641.

[9] J. Fonseca, C. O'Sullivan, M. Coop, P. Lee, Non-invasive characterization of particle morphology of natural sands, Soils and Foundations 52(4): 712-722.

[10] E. Andò, S. A. Hall, G. Viggiani, J. Desrues, P. Bésuelle, Grain-scale experimental investigation of localised deformation in sand: a discrete particle tracking approach, Acta Geotechnica 7 (1) (2012) 1 – 13.

[11] G. Guida, F. Casini, G. M. B. Viggiani, E. Andò, G. Viggiani, Breakage mechanisms of highly porous particles in 1d compression revealed by X-ray tomography, Géotechnique Letters 8 (2) (2018) 155 – 160.

[12] A. M. Druckrey, K. A. Alshibli, 3D finite element modeling of sand particle fracture based on in situ X-ray synchrotron imaging, International Journal for Numerical and Analytical Methods in Geomechanics 40 (1) (2016) 105 – 116.

[13] M. B. Cil, K. A. Alshibli, Modeling the influence of particle morphology on the fracture behavior of silica sand using a 3D discrete element method, Comptes Rendus Mécanique 343(2): 133-142.

[14] A. R. Russell, I. Einav, Energy dissipation from particulate systems undergoing a single particle crushing event, Granular Matter 15 (3) (2013) 299–314.

[15] C. Ovalle, C. Dano, P.-Y. Hicher, Experimental data highlighting the role of surface fracture energy in quasi-static confined comminution, International Journal of Fracture 182 (1) (2013) 123–130.

[16] P. Wang, C. Arson, Energy distribution during the quasi-static confined comminution of granular materials, Acta Geotechnica 13 (5) (2018) 1075–1083.

[17] W. Salim, B. Indraratna, A new elastoplastic constitutive model for coarse granular aggregates incorporating particle breakage, Canadian Geotechnical Journal 41 (4) (2004) 657–671.

[18] A. Daouadji, P.-Y. Hicher, A. Rahma, An elastoplastic model for granular materials taking into account grain breakage, European Journal of Mechanics-A/Solids 20 (1) (2001) 113–137.

[19] M. Cecconi, A. DeSimone, C. Tamagnini, G. MB Viggiani, A constitutive model for granular materials with grain crushing and its application to a pyroclastic soil, International Journal for Numerical and Analytical Methods in Geomechanics 26 (15) (2002) 1531–1560.

[20] G. McDowell, M. Bolton, D. Robertson, The fractal crushing of granular materials, Journal of the Mechanics and Physics of Solids 44 (12) (1996) 2079–2101.

[21] Y. Zhang, G. Buscarnera, A rate-dependent breakage model based on the kinetics of crack growth at the grain scale, Géotechnique (2017) 1–15.

[22] G. D. Nguyen, I. Einav, The energetics of cataclasis based on breakage mechanics, Pure and applied geophysics 166 (10-11) (2009) 1693–1724.

[23] A. Das, A. Tengattini, G. Nguyen, I. Einav, A micromechanics based model for cemented granular materials, Constitutive Modeling of Geomaterials (2013) 527–534.

[24] P. Wang, C. Arson, et al., Breakage mechanics modeling of the brittle-ductile transition in granular materials, in: 50th US Rock Mechanics/Geomechanics Symposium, American Rock Mechanics Association, 2016.

[25] E. G. Ardi, K. Dong, A. Yu, R. Yang, A combined experimental and DEM approach to determine the breakage of particles in an impact mill, Powder Technology 318 (2017) 543–548.

[26] G. Delaney, R. Morrison, M. Sinnott, S. Cummins, P. Cleary, DEM modelling of non-spherical particle breakage and flow in an industrial scale cone crusher, Minerals Engineering 74 (2015) 112–122.

[27] J. Raisianzadeh, A. A. Mirghasemi, S. Mohammadi, 2D simulation of breakage of angular particles using combined DEM and XFEM, Powder Technology 336 (2018) 282 – 297.

[28] N. Jiménez-Herrera, G. K. Barrios, L. M. Tavares, Comparison of breakage models in DEM in simulating impact on particle beds, Advanced Powder Technology 29 (3) (2018) 692–706.

[29] W. L. Lim, G. R. McDowell, Discrete element modelling of railway ballast, Granular Matter 7 (2005) 19–29.

[30] Y. Cheng, Y. Nakata, M. Bolton, Discrete element simulation of crushable soil, Geotechnique 53 (7) (2003) 633–641.

[31] G. McDowell, O. Harireche, Discrete element modelling of soil particle fracture, Géotechnique 52 (2) (2002) 131–135.

[32] T. Ueda, T. Matsushima, Y. Yamada, DEM simulation on the one-dimensional compression behavior of various shaped crushable granular materials, Granular Matter 15 (5) (2013) 675–684.

[33] P. Wang, C. Arson, Discrete element modeling of shielding and size effects during single particle crushing, Computers and Geotechnics 78 (2016) 227–236.

[34] T. Afshar, M. M. Disfani, A. Arulrajah, G. A. Narsilio, S. Emam, Impact of particle shape on breakage of recycled construction and demolition aggregates, Powder Technology 308 (2017) 1–12.

[35] M. O. Ciantia, M. Arroyo, J. Butlanska, A. Gens, DEM modelling of cone penetration tests in a double-porosity crushable granular material, Computers and Geotechnics 73 (2016) 109–127.

[36] J. Wang, H. Yan, DEM analysis of energy dissipation in crushable soils, Soils and Foundations 52 (4) (2012) 644–657.

[37] A. B. Kh, A. Mirghasemi, S. Mohammadi, Numerical simulation of particle breakage of angular particles using combined dem and fem, Powder Technology 205 (1-3) (2011) 15–29.

[38] G. Ma, W. Zhou, X.-L. Chang, Modeling the particle breakage of rockfill materials with the cohesive crack model, Computers and Geotechnics 61 (2014) 132–143.

[39] G. Ma, W. Zhou, X.-L. Chang, M.-X. Chen, A hybrid approach for modeling of breakable granular materials using combined finite-discrete element method, Granular Matter 18 (1) (2016) 7.

[40] G. Ma, W. Zhou, R. A. Regueiro, Q. Wang, X. Chang, Modeling the fragmentation of rock grains using computed tomography and combined fdem, Powder Technology 308 (2017) 388–397.

[41] T. Luo, E. Ooi, A. Chan, S. Fu, The combined scaled boundary finite-discrete element method: Grain breakage modelling in cohesion-less granular media, Computers and Geotechnics 88 (2017) 199–221.

[42] C. Sammis, G. King, R. Biegel, The kinematics of gouge deformation, Pure and applied geophysics 125 (5) (1987) 777 – 812.

[43] O. Tsoungui, D. Vallet, J.-C. Charmet, Numerical model of crushing of grains inside two-dimensional granular materials, Powder Technology 105 (1) (1999) 190 – 198.

[44] Z. Karatza, A study of temporal and spatial evolution of deformation and breakage of dry granular materials using x-ray computed tomography and the discrete element method, Ph.D. thesis, Department of Civil and Environmental Engineering, The University of Edinburgh (2017).

[45] E. Andò, Experimental investigation of micro-structural changes in deforming granular media using x-ray tomography, Ph.D. thesis, Université de Grenoble (2013).

[46] Z. Karatza, E. Andò, S.-A. Papanicolopulos, G. Viggiani, J. Y. Ooi, Evolution of particle breakage studied using x-ray tomography and the discrete element method, EPJ Web Conf. 140 (2017) 07013.

[47] W.-H. Tsai, Document image analysis, IEEE Computer Society Press, Los Alamitos, CA, USA, 1995, Ch. Moment-preserving Thresholding: A New Approach, pp. 44 – 60.

[48] S. Beucher, F. Meyer, The morphological approach to segmentation: the watershed transformation, Mathematical morphology in image processing. Optical Engineering 34 (1993) 433 – 481.

[49] L. Bernard, S. Fave, E. Noirfalise, A. Saragaglia, Visilog 7 Reference Guide: Manual, France: Noesis S.A., 2011.

[50] Z. Karatza, E. Andò, S.-A. Papanicolopulos, J. Y. Ooi, G. Viggiani, Evolution of deformation and breakage in sand studied using X-ray tomography, Géotechnique 68 (2) (2018) 107 – 117.

[51] S. Abe, K. Mair, Grain fracture in 3d numerical simulations of granular shear, Geophysical Research Letters 32 (5).

[52] C. Couroyer, Z. Ning, M. Ghadiri, Distinct element analysis of bulk crushing: effect of particle properties and loading rate, Powder Technology 109 (1-3) (2000) 241–254.

[53] M. Ciantia, M. Arroyo Alvarez de Toledo, F. Calvetti, A. Gens, An approach to enhance efficiency of DEM modelling of soils with crushable grains, Géotechnique 65 (2) (2015) 91–110.

[54] J. de Bono, G. McDowell, Particle breakage criteria in discrete-element modelling, Géotechnique 66 (12) (2016) 1014–1027.

[55] J. Åström, H. Herrmann, Fragmentation of grains in a two-dimensional packing, The European Physical Journal B-Condensed Matter and Complex Systems 5 (3) (1998) 551–554.

[56] O. Ben-Nun, I. Einav, The role of self-organization during confined comminution of granular materials, Philosophical Transactions of the Royal Society of London A: Mathematical, Physical and Engineering Sciences 368 (1910) (2010) 231–247.

[57] K. J. Hanley, C. O'Sullivan, X. Huang, Particle-scale mechanics of sand crushing in compression and shearing using DEM, Soils and Foundations 55 (5) (2015) 1100–1112.

[58] F. Zhu, J. Zhao, A peridynamic investigation on crushing of sand particles, Géotechnique (2018) 1–15.

[59] Y. Hiramatsu, Y. Oka, Determination of the tensile strength of rock by a compression test of an irregular test piece, in: International Journal of

Rock Mechanics and Mining Sciences & Geomechanics Abstracts, Vol. 3, Elsevier, 1966, pp. 89–90.

[60] O. Tsoungui, D. Vallet, J.-C. Charmet, Numerical model of crushing of grains inside two-dimensional granular materials, Powder technology 105 (1) (1999) 190–198.

[61] G. R. McDowell, J. P. de Bono, P. Yue, H.-S. Yu, Micro mechanics of isotropic normal compression, Géotechnique Letters 3 (4) (2013) 166–172.

[62] G. R. McDowell, J. P. de Bono, On the micro mechanics of one-dimensional normal compression, Géotechnique 63 (11) (2013) 895.

[63] S. Lobo-Guerrero, L. E. Vallejo, L. F. Vesga, Visualization of crushing evolution in granular materials under compression using DEM, International Journal of Geomechanics 6 (3) (2006) 195–200.

[64] O. Ben-Nun, I. Einav, A. Tordesillas, Force attractor in confined comminution of granular materials, Physical review letters 104 (10) (2010) 108001.

[65] M. Todisco, W. Wang, M. Coop, K. Senetakis, Multiple contact compression tests on sand particles, Soils and Foundations 57 (1) (2017) 126–140.

[66] M. Lu, G. McDowell, The importance of modelling ballast particle shape in the discrete element method, Granular matter 9 (1-2) (2007) 69–80.

[67] C. Itasca, Pfc 3d-user manual, Itasca Consulting Group, Minneapolis.

[68] M. O. Ciantia, M. Arroyo, F. Calvetti, A. Gens, A numerical investigation of the incremental behavior of crushable granular soils, International Journal for Numerical and Analytical Methods in Geomechanics 40 (13) (2016) 1773–1798.

[69] P. A. Cundall, O. D. Strack, A discrete numerical model for granular assemblies, Geotechnique 29 (1) (1979) 47–65.

[70] Itasca, Particle Flow Code in Three Dimensions, Version 4.0., Itasca Consulting Group, Inc., Minnesota. (2008).

[71] B. Darvell, Uniaxial compression tests and the validity of indirect tensile strength, Journal of Materials Science 25 (l990) (1990) 757–780.

[72] Y. Salami, C. Dano, P.-Y. Hicher, An experimental study on the influence of the coordination number on grain crushing, European Journal of Environmental and Civil Engineering (2017) 1–17.

[73] L. Scholtès, F.-V. Donzé, M. Khanal, Scale effects on strength of geomaterials, case study: coal, Journal of the Mechanics and Physics of Solids 59 (5) (2011) 1131–1146.

[74] Z. P. Bažant, Size effect in blunt fracture: concrete, rock, metal, Journal of Engineering Mechanics.

[75] Y. Ma, H. Huang, Dem analysis of failure mechanisms in the intact brazilian test, International Journal of Rock Mechanics and Mining Sciences 102 (2018) 109–119.

[76] W. Weibull, A statistical theory of the strength of materials, no. 151, Generalstabens litografiska anstalts förlag, 1939.

[77] S. Lobo-Guerrero, L. E. Vallejo, Application of weibull statistics to the tensile strength of rock aggregates, Journal of geotechnical and geoenvironmental engineering 132 (6) (2006) 786–790.

[78] D. Potyondy, P. Cundall, A bonded-particle model for rock, International journal of rock mechanics and mining sciences 41 (8) (2004) 1329–1364.

[79] Y. Xu, C. Xu, Z. Zhou, J. Du, D. Hu, 2D DEM simulation of particle mixing in rotating drum: A parametric study, Particuology 8 (2) (2010) 141–149.

[80] Z. Karatza, E. Andò, S. Papanicolopulos, J. Ooi, G. Viggiani, Evolution of deformation and breakage in sand studied using x-ray tomography, Géotechnique 1 (2017) 1–11.

[81] B. O. Hardin, Crushing of soil particles, Journal of Geotechnical Engineering 111 (10) (1985) 1177–1192.

[82] I. Einav, Breakage mechanics-part i: Theory, Journal of the Mechanics and Physics of Solids 55 (6) (2007) 1274 – 1297.

[83] Z. Karatza, E. Andò, S.-A. Papanicolopulos, G. Viggiani, J. Y. Ooi, Effect of particle morphology and contacts on particle breakage in a granular assembly studied using x-ray tomography, Granular Matter (submitted).